2020 IEEE/RSJ International Conference on Intelligent Robots and Systems (IROS)
October 25-29, 2020, Las Vegas, NV, USA (Virtual)

Evaluating the Efficacy of Parallel Elastic Actuators on High-Speed, Variable Stiffness Running

John V. Nicholson[1], Sean Gart[2], Jason Pusey[2], Jonathan E. Clark[1]

***Abstract*— Although they take many forms, legged robots rely upon springs to achieve high speed, dynamic locomotion. In this paper we examine the effect of adding parallel springs to robots that rely on virtual compliance. Specifically, we consider the trade-off between energetic efficiency and leg versatility that comes while using Parallel Elastic Actuators (PEAs). To do this, we vary the ratio of physical to virtual compliance for legged systems using a) a modified SLIP model, b) a single legged hopping robot, and c) a multibody simulation of the quadruped robot LLAMA. In each case we show that having a small physical compliance significantly improves the efficiency while also maintaining the robot's versatility.**

I. Introduction

Animals in nature locomote through the world by exciting the muscles (*actuators*) in their body which pull on tendons (*springs*) attached to bone structure. This tendon and muscle combination is an intriguing evolution as it provides not only a mechanism for motion but an efficient way to recycle energy passively through the incorporation of passive spring elements. In fact, studies indicate that as much as 50% of the energy for human running is recycled due to spring elements in our legs [1].

The essential role of springs in running has been captured by the Spring-Loaded Inverted Pendulum (SLIP) Model [2], [3]. This sagittal plane, reduced-order dynamic model inspired the design and control of the first [4] and many subsequent legged running robots (e.g. [5]–[7]). One effect of including physical springs in the legs is constrained versatility. The system is limited to a single resonant frequency and leg length at which the robot preforms optimally. Biological systems can overcome this and adapt their limb stiffness by co-contracting antagonistic muscle pairs. There have been many efforts to mimic this functionality by developing Variable Stiffness Actuators (VSA) for robot legs. Some incorporate adjustable mechanical springs [8], [9], others use pairs of antagonistic springs or motors [10], [11], while still others utilize active or smart materials [12], [13]. While effective in isolation, these designs are typically slow, inefficient and/or bulky with few actually fielded on running robots.

Simpler and more reliable solutions featuring a spring in conjunction with a motor, or Series Elastic Actuators [14], have been used in walking machines for years [15], [16]. Recently, interest has developed in using Parallel Elastic Actuators (PEAs) in robotic limbs. Mettin et al. [17] suggested that these may be effective in cyclic tasks, such as running. A few hopping/running robots [18]–[21] were created with PEAs (and even switchable PEAs) in their legs, though none of them evaluated the impact of these springs on their locomotion in the way that we do here. Several simulation studies have evaluated the relative merits of PEAs and SEAs for walking and running [22]–[24]. They show that the use of PEAs should result in energetic advantages at certain frequencies, but these simulation results have not yet been experimentally validated in a running robot.

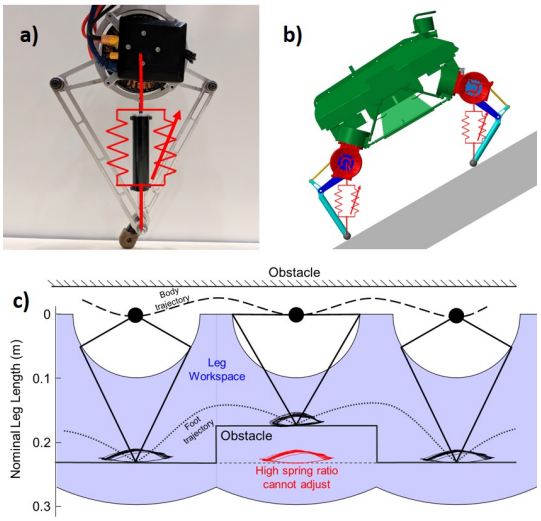

Fig. 1. a) 5-Bar leg used for experiments with spring attachment. b) Simulation of LLAMA. c) Example case of varying ride height while running. In order to maintain a constant center of mass while traversing over a step, the ride height is adjusted accordingly.

Several recently developed robots, such as Minitaur [25], SPOT [26], Cheetah III [27], and LLAMA [28] actuate their linkage system through minimal gear reductions (direct drive) and do not explicitly include physical springs in their leg designs. With little to no gear reduction they achieve mechanical force transparency, enabling these virtual springs to achieve rapid changes of stiffness and rest length, making them very flexible. This variable stiffness should allow effective adaptation to environmental conditions (such as payloads or changes in ground stiffness), while having a variable rest length provides large effective workspaces. The downside of these virtual spring legs is that they are relatively inefficient (motor heat) and power limited (no boost from springs assisting with pushing of leg). Although not yet implemented, these robots could be ideal candidates for the

[1] J. Nicholson and J. Clark are with Mechanical Engineering, Florida A&M University-Florida State University
[2] S. Gart and J. Pusey are with the Army Research Laboratory

inclusions of PEAs.

In this paper we examine how introducing PEAs and changing the ratio of physical and virtual stiffness affects the *efficiency* and *versatility* of a pair of high-speed, variable stiffness running robots (see Fig. 1a,b). While the potential energetic advantages are well known, the drawbacks to versatility of adding parallel physical springs are less well understood. To what extent will these springs reduce the usable workspace of the robot? Will they lock the robot into a limited range of natural frequencies, or limit the range of locomotive behaviors such as running in a low ride-height (crouching gait) or shortening the leg to stepping on an obstacle (both of which are shown in Fig. 1c). In this paper we consider three metrics as proxies for versatility: varied desired ride height, response to an increase in payload, and climbing slopes. These, respectively, capture the effect of workspace reduction, resonant frequency locking, and behavioral limits.

The remainder of the paper is organized as follows: Sec. II introduces the PEA SLIP-like hopping model. The simulated response of the hopper to changes in leg stiffness, ratio of mechanical to virtual springs, and ride height are outlined in Sec. III. The leg design and experimental setup for the Minitaur leg are described in Sec. IV, and Sec. V outlines the experimental results of running with different physical springs and payloads. Section VI describes the application of PEAs on the quadruped LLAMA. The paper concludes (Sec. VII) with directions for future work.

II. Simulation

A. Hopping Model

To simulate the Minitaur leg shown in Fig 1a, a modified SLIP model is used. This model has been adapted to include two springs in parallel, as seen in Fig. 2a. One spring is assumed to be a physical element P, and the other a virtual element V. The nominal length and stiffness of each spring is dependent on its type and location on the five-bar leg. Potential types and locations are denoted by k_1, k_2, and k_3 as a torsional spring at the hip, a pair of torsional springs at the knees, and a linear spring along the leg, respectively, as shown in Fig. 2b. The physical spring element is assumed to restore all energy, with no damping elements. The virtual spring is assumed to store no energy, such that any force generated is the result of actuation. The links, with lengths λ_1 and λ_2, are assumed to remain constant throughout this study and possess no mass. The robot body is defined as a point mass, while the foot is assumed to have sufficient friction to avoid sliding when contacting the ground. All motion is constrained within the sagittal plane.

The motion of the modified SLIP model is defined by two sets of equations, one set for the stance phase, while the leg is in contact with the ground, and one set for the flight phase. The stance phase equations are defined as

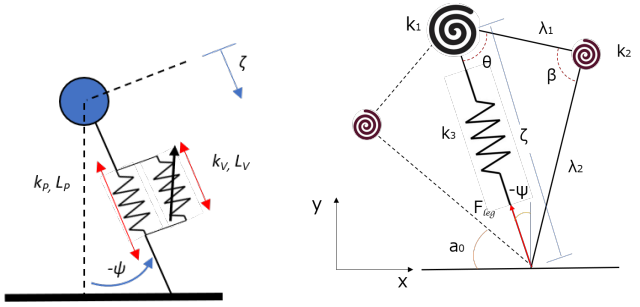

Fig. 2. a) Diagram of the modified SLIP model used to study the effect of multiple springs. Each spring can utilize a different nominal length and stiffness. One spring is defined to be a virtual spring V, while the other is defined to be a physical spring P. The length and angle of the leg are ζ and ψ, respectively. b) Diagram of the 5-bar leg simulated by the modified SLIP Model. The leg can include springs at 3 possible locations, labeled as k_1, k_2, and k_3

TABLE I
Model Parameters

Parameters	Symbols	Robot Values	Units
Spring Stiffness	k_{ref}	25	N/A
Stiffness Ratio	k_{ratio}	[0:2.5:100]	(%)
Phys Spring Stiff	k_P	Eq. 8	N/A
Virt Spring Stiff	k_V	Eq. 8	N/A
Nominal Phys Length	L_P	0.23	(m)
Nominal Virt Length	L_V	0.23	(m)
Ride Height	L_{nom}	Eq. 9	(m)
Thrust Factor	C_{thrust}	40	(%)
Actuator Damping	b_m	0.088	$(Nm * s/rad)$
Touchdown Angle	ψ_{TD}	[0:30]	(°)
Mass	m	1.55	(kg)
Gravity	g	9.81	(m/s^2)
Length Scale Factor	α_L	$L_{nom}/1$	(m)
Launch Height	y_{apex}	$1 * \alpha_L$	(m)
Input Velocity	v_x	$5.0 * \alpha_L$	(m/s)
Segment 1	λ_1	0.1	(m)
Segment 2	λ_2	0.2	(m)
Motor Model			
Stall Torque	τ_S	5.92	(Nm)
No Load Speed	W_{NL}	157	(rad/s)
Gear Ratio	GR	1	N/A
Torque Constant	K_t	0.075	N/A
Winding Resistance	R_m	0.19	(Ω)

$$\begin{cases} \ddot{\zeta} = \zeta\dot{\psi}^2 - g\cos(\psi) + \dfrac{F_P}{m} + \dfrac{F_V}{m} - J_M^{-T}\dfrac{b_M}{m}J_M^{-1}\dot{\zeta} \\ \ddot{\psi} = -\dfrac{2\dot{\zeta}\dot{\psi}}{\zeta} + \dfrac{g}{\zeta}\sin(\psi) - \dfrac{b_M}{m\zeta^2}\dot{\psi} \end{cases} \tag{1}$$

where ζ is leg length, ψ is leg angle, g is gravity, m is mass, and F is spring force. The subscripts P and V indicate the physical and virtual elements, respectively. The damping from the motors is represented by b_M, and J_M is the kinematic Jacobian for the actuator. For the symmetric 5-bar leg design shown the actuator Jacobian will be $J_M = J_2$. the spring forces can be further written as

$$F_P = -k_P J_P^{-T}(L_P - \zeta_P) - b_P\dot{\zeta} \tag{2}$$

$$F_V = \begin{cases} -k_V J_V^{-T}(L_V - \zeta_V), \text{if } \dot{\zeta} < 0, \\ -k_V J_V^{-T}(L_V - \zeta_V) - \tau_S(C_{Thrust})J_M^{-T}, \text{if } \dot{\zeta} \geq 0, \end{cases} \tag{3}$$

where k and L represent the spring stiffness and nominal

length, and J represents the kinematic Jacobian. In stance, a fixed thrust offset is applied after maximum compression for the remaining duration of stance. The fixed thrust offset is defined with τ_S, stall torque of the actuators, and C_{Thrust}, the percentage of that stall torque used to jump. The Jacobian is utilized to transform the force or torque generated by a spring into the resultant forces within the SLIP model. Its expression is dependent on the type and location of the spring on the 5-bar leg and is defined as

$$\begin{cases} F = (J_i^T)^{-1}\tau, i = 1, 2, 3. \\ J_1 = -\dfrac{\lambda_1^2 \sin(\theta) cos(\theta)}{\sqrt{\lambda_2^2 - (\lambda_1 \sin(\theta))^2}} - \lambda_1 \sin(\theta) \\ J_2 = -\dfrac{\lambda_1 \lambda_2}{\zeta} \sin(\beta) \\ J_3 = 1 \end{cases} \tag{4}$$

The flight phase equations are defined as

$$\begin{cases} \ddot{x} = 0 \\ \ddot{y} = -g \end{cases} \tag{5}$$

with x, y representing the horizontal and vertical positions of the body, respectively. The touchdown event occurs at

$$y = \zeta_{eq} \cos(\psi_{TD}), \tag{6}$$

where ζ_{eq} is the equilibrium length of the leg, dependent on the rest length and stiffness of each spring and ψ_{TD} is the touchdown angle of the leg. The lift off event occurs at

$$\begin{cases} \sum F_y = 0 \\ \dot{\zeta} > 0 \end{cases} \tag{7}$$

or when the forces in the y direction sum to zero and the change in leg length $\dot{\zeta}$ is positive.

To define the total stiffness of the physical and virtual spring, we first set a nondimensional reference stiffness, $\tilde{k}_{ref}$. This value defines the relative stiffness of the system assuming a 10% compression of the leg as defined in [29]. The total stiffness is then split between the physical and virtual springs by a stiffness ratio, k_{ratio}, and converted to the proper dimensions of that spring, given by

$$\begin{cases} k_P = k_{ratio} \tilde{k}_{ref} \\ k_V = (1 - k_{ratio}) \tilde{k}_{ref} \end{cases} \tag{8}$$

Since there are two springs used on the leg, the nominal length is no longer simple to define. The nominal length of the leg can vary based on the stiffness and rest length of each spring. The resultant nominal leg length can be found from the relation

$$F = \frac{k_P}{m} J_P^{-T}(L_P - \zeta_P) + \frac{k_V}{m} J_V^{-T}(L_V - \zeta_V) \tag{9}$$

When the leg is at equilibrium the resultant force in the leg becomes $F = 0$, and solving for ζ will result in the nominal length of the leg, L_{nom}. The parameters utilized in the model are summarized in Table I.

B. Stability Analysis

To determine a set of running parameters, the system stability was evaluated utilizing eigenvalues of the linearized Poincare map at apex height of a periodic gait. A periodic gait, or fix point, of the system can be described by two parameters, the height of the body in flight y_{apex} and the forward velocity v_x. For eigenvalues larger than 1, the system becomes unstable, while gaits with an eigenvalue of 1 are neutrally stable and eigenvalues lower than 1 are stable. The fixed points were found utilizing a Newton-Raphson based approach. For this study the initial conditions of the search will be a scaled down version of human running parameters, with a forward velocity of $v_x = 5.0\alpha_L^{1/2}$ m/s and a apex height of $y_{apex} = \alpha_L$ m, where $\alpha_L = L_{nom}$ [30], [31].

C. Power Analysis

To simulate a virtual spring effectively, an actuator model of the brushless DC motors was needed. This allows us to study how much energy is consumed by the actuators during locomotion. For this study the actuator specifications are defined using the T-Motor U-8 actuators used in the Minitaur platform. The torque τ of the DC motor model used in the simulation is given by

$$\tau = \tau_S - \omega \, \tau_S / W_{NL}, \tag{10}$$

where ω is the angular velocity, $\tau_S = 5.92Nm$ is the stall torque, and $W_{NL} = 157rad/s$ is the no load speed. The power consumption P is given by

$$P = \omega\tau + \left(\frac{\tau}{K_t}\right)^2 R_m, \tag{11}$$

and includes both the mechanical power (1st term) and the power loss due to heat (2nd term). A list of motor properties can be found in Table I. For a metric of efficiency the Cost of Transport (COT) will be used. The COT is given by

$$COT = \frac{P}{mgv} \tag{12}$$

To evaluate the modified SLIP model, we performed simulations using ode45 in MATLAB. The precisions of the solver were set to $abstol = 10^{-10}$ and $reltol = 10^{-10}$.

III. Simulation Results and Discussion

A. Spring Selection

To assess how each spring design behaves, an initial sweep of spring ratio from 0% (no physical spring) to 100% (all physical spring) and touchdown angle from 0° to 20° was run using leg parameters given in Table I. The nominal leg length, or ride height, was chosen based on previous results [32], the nominal length of virtual and physical leg was set to 23 cm. The resultant Costs of Transport for the three springs: torsional hip k_1, torsional knee k_2, and linear hip k_3, can be seen in Fig. 3.

The similarities in the resulting COT values and range of stable touchdown angles suggest that all of the spring locations behaved in a similar fashion, with marginal changes when the motors began to reach stall torque conditions.

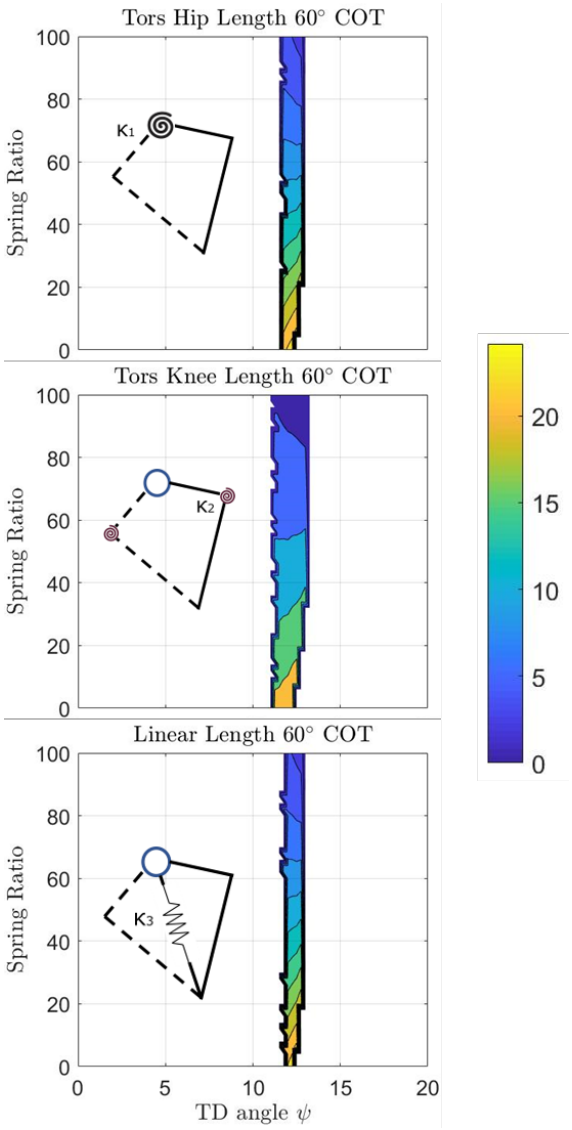

Fig. 3. Each figure represents a different spring type as seen in Figure 2. The virtual rest length and the physical rest length is held constant at $L_P = L_V = 0.23$ m, and the stiffness is held at $\tilde{k}_{ref} = 25$. The touchdown angle ψ_{TD} and spring ratio k_{ratio} are then swept to get an understanding of the design space for each configuration. Regions with stable running gaits are mapped to each plot, with the color map indicating the Cost of Transport (COT).

As compliance is shifted from a purely virtual element, a spring ratio of $k_{ratio} = 0$, to a purely physical element, $k_{ratio} = 100$, the cost of transport is significantly reduced. The low variance between the locations suggests that choice of spring placement does not yield any significant benefits or losses. In terms of design, this suggests that convenient spring placement is likely a more important consideration than enforcing a specific spring into the kinematics. With this in mind further simulation tests will be done using simply the linear hip spring design, k_3.

B. Overall Leg Stiffness Variation

To show the effect of overall leg stiffness while using PEAs, three physical springs were selected, $k_P = 0$, 5, and 10. Then, a sweep of virtual stiffness k_V = [0:0.5:25] and touchdown angle was performed in simulation, giving a total range of $\tilde{k}_{ref} = 0$ to 35. The resulting costs of transport are presented in Fig. 4. As seen in previous works [32], when the overall stiffness of the legged system is increased the touchdown angle decreases. In order to achieve stable gaits a minimum, non-dimensional, total stiffness of $\tilde{k}_{ref} = 5$ is needed.

When comparing these plots, the effect of added physical compliance is again shown to increase the system's efficiency. Simply adding a physical spring as small as k_V 5, can reduce the overall cost of transport by roughly 30% from a purely virtual spring. Although a stiffer spring may improve efficiency more, softer springs allow for a larger range of achievable overall stiffness within the limitations of the actuators that form the virtual spring. A more diverse stiffness range is critical to producing legs with a high degree of locomotive versatility.

C. Ride Height Variation

Fig. 5 shows the resulting (inverted) cost of transport and ride heights that can be achieved for various k_{ratio}.

Consistent with previous trials, increased spring ratio (% of physical spring) yields a more efficient robot, as seen by the increased values of the inverted cost of transport. As a tradeoff, the realizable ride heights are reduced significantly, with the 100% spring ratio being limited to a single height. It appears that using spring ratios of 20-40% maintains the benefits of reduced overall Cost of Transport while giving more versatility than the no spring case.

In summary, when running at the ideal length, using only a physical spring yields the most energy efficient result. Location of the physical spring does not appear to matter, but there needs to be some mechanical compliance within the leg, at a minimum $\tilde{k}_{ref} = 5$. When moving away from the nominal leg length, having a small amount of physical stiffness k_{ratio} = 20-40% significantly improves the versatility of the leg, while still receiving benefits to energy efficiency.

IV. Experimental Setup

A. Leg and Boom Design

To validate these simulations, an experimental platform was developed with a single, direct drive 5-bar linkage leg from Minitaur [33] powered by two T-motor U8 brushless motors. To restrict the leg motion to the sagittal plane, the leg is attached to a 1.34 m boom arm. The touchdown point (toe) is made of 3D printed ABS plastic with an overmolded elastomer to increase friction between the ground and the leg as seen in Fig. 2c. Parameters for this design can be seen in Table I.

To calculate motor power, Eq. 11, the desired motor torque τ from the leg and motor measured angular velocity ω from the motor's Hall Effect based absolute encoders are used. To measure horizontal speed, v, an Encoder Outlet model 15s rotary encoder operating in quadrature phase was used. Data is recorded at 1000 Hz with a Teensy 3.6 microcontroller.

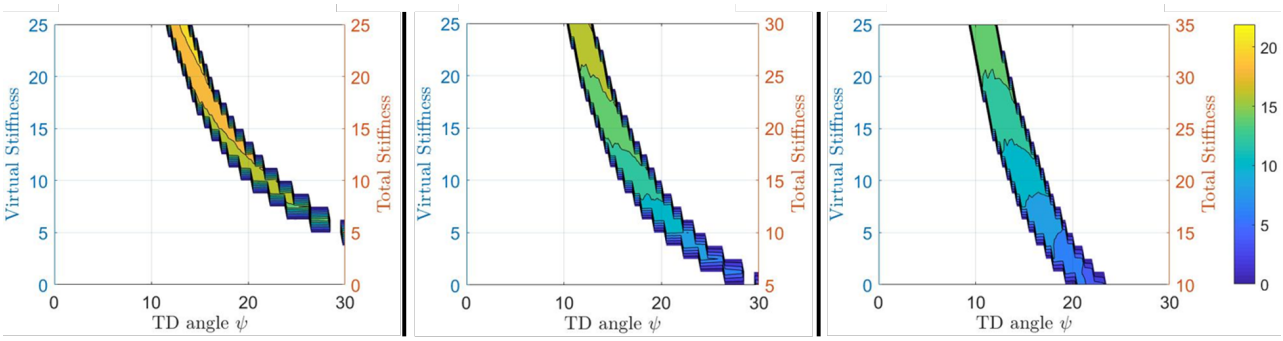

Fig. 4. Each figure represents a different physical stiffness ranging from k_P = [0,5,10]. To evaluate using variable compliance with the leg, the virtual stiffness k_V is swept from 0 to 25 on the vertical axis, with touchdown angle as the horizontal axis. Cost of transport is used as the color map.

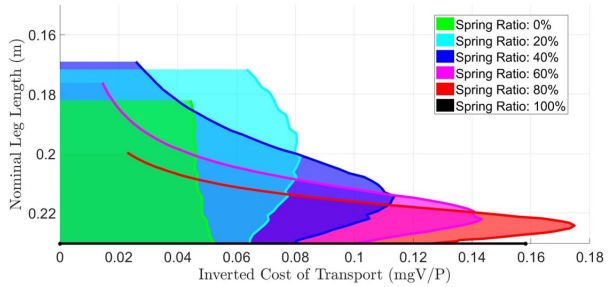

Fig. 5. Using a physical spring with length $L_P = 0.23m$ and a touchdown angle of $\psi_{TD} = 12°$, a sweep of different leg configurations was tested. With different spring ratios and virtual lengths L_V, various ride heights with different COT can be achieved depending on the tasks required. The Shaded regions denote the available ride heights for a given spring ratio, and how efficient those ride heights are as the curve shifts from left to right along the inverted cost of transport axis.

B. Spring Design

The passive compressive spring element fixed between the hip and toe was encapsulated within a cylindrical housing. One end of the cylinder was fixed to the ankle and a spring placed inside was compressed by a piston and rod assembly that protruded from a cap on the other end of the cylinder. The plunging rod was attached to an assembly mounted between the two motors. Both ends of the spring assembly constricted the change in distance between the ankle and hip to compress the spring. The cylindrical housing contained a large breather hole, allowing air to escape, preventing large damping forces within the spring fixture. Springs ranging of 322, 644, and 1278 N/m were used for spring ratios of 20%, 40%, and 80% respectively and are able to be swapped out during physical testing. The rest length of the physical spring can be altered using the threaded rods and lock nuts at the hip and toe of the leg.

C. Running Controller

Because the leg does not have a physical switch on the toe and the parallel physical spring affects the forces on the motors, it was necessary to implement a position based condition to detect liftoff and touchdown conditions. During stance, the angular controller was set to be passive. In flight, a PD controller was used to reset the leg to the specified touchdown angle. The equation for thrust generated by the actuators is given by Eq. 3.

D. Experimental Methods

For each test, the 5-bar leg was run a distance of 4.25 m around the circular track, thrown by a human operator to achieve a reasonable initial forward velocity. The physical spring was designed to have a nominal length of L_P = 0.23m for all experiments in the study. Unless otherwise specified, each leg configuration was designed to have a relative stiffness $\tilde{k}_{ref}$ = 25. Five trials were run for each parameter variation. To eliminate transient effects, the first and last two strides for each run were removed from the analysis. The fixed thrust value was set to 40% of the stall torque of the actuators in all trials. For each setting, touchdown angles from $10 - 20$ degrees were tested to identify stable gaits. For testing with added payload, a weight of 0.5 kg was mounted to the top of the leg.

V. Experimental Results and Discussion

Two experiments were performed using the 5-bar leg. The first set of experiments were designed to verify the ride height results found in III-C. The second set of experiments look into the addition of a payload onto the platform, a case where we expect [34] that a variable stiffness leg will help preserve the resonant system frequency.

A. Ride Height Variation

The versatility of the system, measured by its ability to alter ride height, was tested on the experimental platform using four spring ratios, k_{ratio} = [0, 20, 40, 80]%. A touchdown angle of $\psi_{TD} = 12°$ was used for all tests. For each spring ratio, the virtual length was first set to L_V = 0.23 m. The nominal leg length L_{nom} was decreased by 0.005 m for each subsequent trial until failure occurred. Fig. 6 shows the resulting experimental ride height capability for each spring ratio. For a ride height of 0.23 m, as the spring ratio on the leg increases the efficiency also increases, with an increase in inverted COT by 100% (or reduction of 50% in COT). This agrees with the simulation results shown in Fig. 4. Similar to Fig. 5, as the spring ratio goes down,the range of achievable ride heights increases. Once the 0% (purely virtual) spring's ride height was reduced below

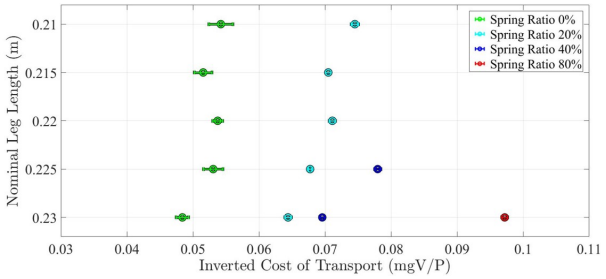

Fig. 6. Experimental Results: Cost of transport (COT) as a function of ride height for 0%, 20%, 40%, and 80% spring ratios. Only configurations with stable gaits are displayed.

21cm, the gait became unstable. Motor saturation resulted in inconsistent running and large COT variance. At the nominal (0.23 m) height for the 20% spring ratio the Cost of Transport was reduced by 38% As predicted by the simulation, the power gain from using the 20% physical spring allowed it to outperform the purely virtual spring while maintaining the same level of versatility. It is worth noting the 20% spring ratio began to fail at smaller ride heights due to limitations of the physical spring device's maximum compression rather than by power limits or becoming unstable.

B. Stiffness Variation

To test the variable stiffness legs' capability to adapt to changes in the robot's environment, a soft physical spring with stiffness k_P = 5 was selected and tested with two different virtual springs settings, soft and stiff, where k_V = [5, 20]. Each configuration was tested both with and without a 0.5 kg payload. Table II details the COT and velocity of each configuration. Without the payload, the soft spring was the more efficient gait, with a 60% reduction in COT, consistent with the findings seen in Figure 4. The soft spring had a larger touchdown angle as well, a 19° angle versus a 12° angle for the hard spring, again matching the simulation prediction. With the added 0.5 kg payload, the soft spring could no longer achieve stable running. The stiff spring not only supported the added payload for a small increase in COT, but also adapted to a gait similar to the soft spring without the payload, matching both touchdown angle and forward velocity.

TABLE II
RESULTS FROM PAYLOAD TEST

	No Payload 1.55 kg		Payload 2.05 kg	
Soft $\tilde{k}_{ref} = 10$	COT:	5.9 ± 0.02	COT:	DNR
$K_P = 5$	Vel:	1.3 ± 0.01	Vel:	DNR
$K_V = 5$	TD:	19°	TD:	DNR
Stiff $\tilde{k}_{ref} = 25$	COT:	14.8 ± 0.8	COT:	16.2 ± 0.7
$K_P = 5$	Vel:	1.1 ± 0.05	Vel:	1.3 ± 0.06
$K_V = 20$	TD:	12°	TD:	19°

VI. PEAs ON A QUADRUPED

Simulation environments also allow us to study more complex robot designs outside of the SLIP model. In addition, we can evaluate other situations where versatility would be useful, such as walking up inclines. By using a different robot and linkage morphology from Figure 2b, we also show that different leg designs and platforms can benefit from PEAs.

A. Quadruped Model

To extend our study of the tradeoffs of PEAs on the versatility and energetic efficiency of running we consider the quadruped robot LLAMA (Fig 1b) for which we have recently developed a multibody simulation using Simscape Multibody [28]. Like Minitaur, LLAMA currently relies on purely virtual springs in its legs. We modified the simulation to include a linear spring element attached from the hip to the toe. The nominal length of the spring is defined as the touchdown length of the trajectory, L_{Spring}. The stiffness of the physical spring is defined using the spring ratio (Eq.8) and the overall linear stiffness of the LLAMA legs. The parameters used for the compliant leg testing can be seen in Table III.

TABLE III
COMPLIANT LEG PARAMETERS

Leg Parameters			
Parameter	Symbol	Value	Units
Spring Rest Length	L_{Spring}	0.40753	(m)
Spring Stiffness	k_{ref}	16000	(N/m)
Phys Spring Stiff	K_P	Eq. 8	(N/m)
Virt Spring Stiff	K_V	Eq. 8	(N/m)
Flight Stiffness	K_{FL}	16000	(N/m)

B. Quadruped Running

To test the compliant leg, the spring ratio was swept from 0-100% while the robot ran on a flat surface. The results can be seen in Fig. 7 as the 0°(blue solid line) case. The controller nominally ran at an average speed of 1.64 m/s with an average power consumption of 1489 W per stride at steady state for the case, resulting in a cost of transport of 1.112. The introduction of a 40% physical spring reduced the COT by 25% without any additional tuning. Using PEAs on flat terrain results in a significant reduction of power consumption during the stance phase of each stride with significant diminishing returns after passing over spring ratios of 40%. The power required to recirculate the leg in flight increases, however, as the physical spring restricts the motion of the foot. Similar to the results found in Section III and Section III-C, using a spring ratio of 20-40% results in a significant reduction of power consumption during stance while having only a small increase in power consumed during flight for running on flat terrain.

C. Quadruped on Slopes

To evaluate the limitations that PEAs have on the versatility of the leg, LLAMA was studied running on various inclined planes. In order to properly traverse the slopes, the posture of the robot was adjusted to keep the body parallel to the slope while keeping the legs aligned with gravity. In addition, changes to the leg trajectory were also made to

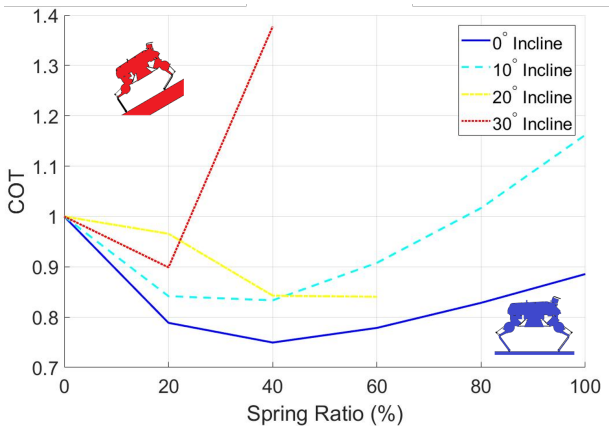

Fig. 7. The effect of spring ratio on the quadruped robot while running on inclined terrain, in terms of normalized COT. LLAMA is able to walk on inclines of up to 30°, with PEAs of 20-40% still being usable and even improving performance. Higher spring ratios struggle due to working outside of their intended configurations.

help achieve stable gaits. This includes adjusting the stride frequency to maintain stability of the legs and for larger inclines (slopes of 30°and greater) to reduce the stroke length of the legs. To maintain consistency the physical spring elements used in these tests will match the same parameters used in Section VI-B.

The baseline ($k_{ratio} = 0$) cost of transport increases with each incline, with COT = 1.11, 1.50, 3.18, and 6.13 for inclines of 0°, 10°, 20°, and 30°case, respectively. To improve visibility of the results, COT in Fig. 7 is normalized about $k_{ratio} = 0$ and shows the results of LLAMA traversing inclines of up to 30°. LLAMA is able to achieve stable walking on up to 30°inclines, while still utilizing the PEAs. As expected, the larger spring ratios end up performing worse on inclines, since the stiffer systems resulted in reduced motion of the legs and increased power consumption. The lower spring ratios however, were not only able to handle inclines but even improved performance of the robot on all slopes.

VII. Conclusions and Future Work

Simulation and experimental results of LLAMA and the Minitaur 5-bar leg have demonstrated some of the trade-offs inherent between efficiency and versatility in running with a variable stiffness Parallel Elastic Actuator configuration. Specifically, we have shown that the location and type of physical spring (be it prismatic, rotational, between the hips, feet, or knees) did not have much of an impact on the resulting COT. The dramatic energetic savings predicted by previous work can be found as long as the PEA is used at the optimal (nominal) configuration. This was found for two different leg kinematics for two very different robots. We have also found that, while the versatility of a PEA with a large physical spring is much lower than a purely virtual spring, surprisingly a light (in our case about 20%) physical spring can actually improve versatility, both in terms of achievable ride height and ability to traverse inclines. Lastly, we have physically demonstrated using a variable stiffness PEA to adapt to changing environmental conditions (payload) to avoid unstable/falling behavior. Future work includes extending this study to include series springs, physical implementation on a quadrupedal platform such as Minitaur or LLAMA, and optimizing its efficiency. In addition, we are interested in evaluating the performance of PEAs in real, unstructured terrain.

Acknowledgments

This work was supported by Cooperative Agreement DAAD 19-01-2-0012. The U.S. Government is authorized to reproduce and distribute reprints for Government purposes not withstanding any copyright notation thereon. Thanks to Charles Young for help with setup of the experimental platform.

References

[1] R. M. Alexander, *Principles of animal locomotion*. Princeton University Press, 2003.

[2] G. A. Cavagna, N. C. Heglund, and C. R. Taylor, "Mechanical work in terrestrial locomotion: two basic mechanisms for minimizing energy expenditure," *American J. of Physiology-Regulatory, Integrative and Comparative Physiology*, vol. 233, no. 5, pp. R243–R261, 1977.

[3] R. Blickhan, "The spring-mass model for running and hopping," *J. of Biomechanics*, vol. 22, no. 11-12, pp. 1217–1227, 1989.

[4] M. Raibert, M. Chepponis, and H. Brown, "Running on four legs as though they were one," *IEEE J. on Robotics and Automation*, vol. 2, no. 2, pp. 70–82, Jun 1986.

[5] I. Poulakakis, J. A. Smith, and M. Buehler, "Modeling and experiments of untethered quadrupedal running with a bounding gait: The scout ii robot," *Int'l J. of Robotics Research*, vol. 24, no. 4, pp. 239–256, 2005.

[6] U. Saranli, M. Buehler, and D. E. Koditschek, "Rhex: A simple and highly mobile hexapod robot," *Int'l J. of Robotics Research*, vol. 20, no. 7, pp. 616–631, Jul. 2001.

[7] J. Cham, S. Bailey, J. Clark, R. Full, and M. Cutkosky, "Fast and robust: Hexapedal robots via shape deposition manufacturing," *Int'l J. of Robotics Research*, vol. 21, no. 10, pp. 869–882, 2002.

[8] K. Galloway, J. Clark, M. Yim, and D. Koditschek, "Experimental investigations into role of passive variable compliant legs for dynamic robotic locomotion," in *IEEE Int'l Conf. on Robotics and Automation*.

[9] V. Ham, T. Sugar, B. Vanderborght, K. Hollander, and D. Lefeber, "Compliant actuator designs: Review of actuators with passive adjustable compliance/controllable stiffness for robotic applications," *IEEE Robotics and Automation Mag.*, vol. 16, no. 3, pp. 81–94, 2009.

[10] J. W. Hurst, J. E. Chestnutt, and A. A. Rizzi, "An actuator with physically variable stiffness for highly dynamic legged locomotion," in *Robotics and Automation, 2004. Proc. ICRA'04. 2004 IEEE Int'l Conf. on*, vol. 5. IEEE, 2004, pp. 4662–4667.

[11] B. Vanderborght, A. Albu-Schäffer, A. Bicchi, E. Burdet, D. G. Caldwell, R. Carloni, M. G. Catalano, O. Eiberger, W. Friedl, G. Ganesh, M. Garabini, M. Grebenstein, G. Grioli, S. Haddadin, H. Höppner, A. Jafari, M. Laffranchi, D. Lefeber, F. Petit, S. Stramigioli, N. G. Tsagarakis, M. V. Damme, R. V. Ham, L. C. Visser, and S. Wolf, "Variable impedance actuators: A review," *Robotics and Autonomous Systems*, vol. 61, pp. 1601–1614, 2013.

[12] D. Haldane and J. Clark, "Design of a variable stiffness leg using shape meory polymer composites," Johns Hopkins Univ., USA, July 2012.

[13] M. D. Christie, S. S. Sun, D. H. Ning, H. Du, S. W. Zhang, and W. H. Li, "A torsional MRE joint for a c-shaped robotic leg," *Smart Materials and Structures*, vol. 26, no. 1, p. 015002, nov 2016.

[14] G. A. Pratt and M. M. Williamson, "Series elastic actuators," in *Proc. 1995 IEEE/RSJ Int'l Conf. on Intelligent Robots and Systems. Human Robot Interaction and Cooperative Robots*, vol. 1, Aug 1995, pp. 399–406 vol.1.

[15] J. Pratt and G. Pratt, "Intuitive control of a planar bipedal walking robot," in *Proc. 1998 IEEE Int'l Conf. on Robotics and Automation (Cat. No.98CH36146)*, vol. 3, May 1998, pp. 2014–2021 vol.3.

[16] N. Paine, J. S. Mehling, J. Holley, N. A. Radford, G. Johnson, C.-L. Fok, and L. Sentis, "Actuator control for the nasa-jsc valkyrie humanoid robot: A decoupled dynamics approach for torque control of series elastic robots," *J. of Field Robotics*, vol. 32, no. 3, pp. 378–396, 2015. [Online]. Available: https://onlinelibrary.wiley.com/doi/abs/10.1002/rob.21556

[17] U. Mettin, P. X. L. Hera, L. B. Freidovich, and A. S. Shiriaev, "Parallel elastic actuators as a control tool for preplanned trajectories of underactuated mechanical systems," *Int'l J. of Robotics Research*, vol. 29, no. 9, pp. 1186–1198, 2010. [Online]. Available: https://doi.org/10.1177/0278364909344002

[18] F. Günther, Y. Shu, and F. Iida, "Parallel elastic actuation for efficient large payload locomotion," in *2015 IEEE Int'l Conf. on Robotics and Automation (ICRA)*, May 2015, pp. 823–828.

[19] I. Wanders, G. Folkertsma, and S. Stramigioli, "Design and analysis of an optimal hopper for use in resonance-based locomotion," in *2015 IEEE Int'l Conf. on Robotics Automation*, May 2015, pp. 5197–5202.

[20] J. G. D. Karssen, M. Haberland, M. Wisse, and S. Kim, "The effects of swing-leg retraction on running performance: analysis, simulation, and experiment," *Robotica*, vol. 33, no. 10, p. 2137–2155, 2015.

[21] X. Liu, A. Rossi, and I. Poulakakis, "A switchable parallel elastic actuator and its application to leg design for running robots," *IEEE/ASME Trans. on Mechatronics*, vol. 23, no. 6, pp. 2681–2692, Dec 2018.

[22] G. A. Folkertsma, S. Kim, and S. Stramigioli, "Parallel stiffness in a bounding quadruped with flexible spine," in *2012 IEEE/RSJ Int'l Conf. on Intelligent Robots and Systems*, Oct 2012, pp. 2210–2215.

[23] M. A. Sharbafi, M. J. Yazdanpanah, M. N. Ahmadabadi, and A. Seyfarth, "Parallel compliance design for increasing robustness and efficiency in legged locomotion-proof of concept," *IEEE/ASME Trans. on Mechatronics*, 2019.

[24] Y. Yesilevskiy, Weitao Xi, and C. D. Remy, "A comparison of series and parallel elasticity in a monoped hopper," in *2015 IEEE Int'l Conf. on Robotics and Automation (ICRA)*, May 2015, pp. 1036–1041.

[25] G. Kenneally, A. De, and D. E. Koditschek, "Design principles for a family of direct-drive legged robots," *IEEE Robotics and Automation Letters*, vol. 1, no. 2, pp. 900–907, July 2016.

[26] E. Guizzo, "By leaps and bounds: An exclusive look at how boston dynamics is redefining robot agility," *IEEE Spectrum*, vol. 56, no. 12, pp. 34–39, 2019.

[27] G. Bledt, M. J. Powell, B. Katz, J. Di Carlo, P. M. Wensing, and S. Kim, "Mit cheetah 3: Design and control of a robust, dynamic quadruped robot," in *2018 IEEE/RSJ International Conference on Intelligent Robots and Systems (IROS)*. IEEE, 2018, pp. 2245–2252.

[28] M. Y. Harper, J. V. Nicholson, E. G. Collins, J. Pusey, and J. E. Clark, "Energy efficient navigation for running legged robots," in *2019 Int'l Conf. on Robotics and Automation (ICRA)*, May 2019, pp. 6770–6776.

[29] J. Rummel and A. Seyfarth, "Stable running with segmented legs," *Int'l J. of Robotics Research*, vol. 27, no. 8, pp. 919–934, 2008. [Online]. Available: https://doi.org/10.1177/0278364908095136

[30] S. Riese and A. Seyfarth, "Stance leg control: variation of leg parameters supports stable hopping," *Bioinspiration & biomimetics*, vol. 7, no. 1, p. 016006, 2011.

[31] B. D. Miller and J. E. Clark, "Dynamic similarity and scaling for the design of dynamical legged robots," in *2015 IEEE/RSJ Int'l Conf. on Intelligent Robots and Systems (IROS)*. IEEE, 2015, pp. 5719–5726.

[32] D.J.Blackman, J.V.Nicholson, J.L.Pusey, M.P.Austin, C.Young, J.M.Brown, and J.E.Clark, "Leg design for running and jumping dynamics," in *2017 IEEE Int'l Conf. on Robotics and Biomimetics (ROBIO)*, Dec 2017, pp. 1–6.

[33] G. Kenneally and D. E. Koditschek, "Leg design for energy management in an electromechanical robot," in *2015 IEEE/RSJ Int'l Conf. on Intelligent Robots and Systems (IROS)*, Sept 2015, pp. 5712–5718.

[34] J. Y. Jun and J. E. Clark, "Dynamic stability of variable stiffness running," in *2009 IEEE Int'l Conf. on Robotics and Automation*, May 2009, pp. 1756–1761.